HYDROACOUSTICS
4, 181-192 (2001)

ANOMALOUS LOW FREQUENCY SEA SURFACE REVERBERATION

T. H. Neighbors
Science Applications International Corporation, 1710 SAIC Drive, MS-1-3-8
McLean, Virginia 22101, USA
Thomasneig@cs.com
L. Bjørnø
UltraTech Holding, Stendiget 19, DK-2630 Taastrup, Denmark
prof.lb@get2net.dk

Low frequency sea surface sound backscattering from ~100 Hz to a few kHz observed from the 1960s [A,B,C] to the 1990s [D,E] is substantially higher than explained by rough sea surface scattering theory. Alternative theories for explaining this difference range from scattering by bubble plumes/clouds formed by breaking waves to stochastic scattering from fluctuating bubble layers. Disparities remain between measurements and predictions [F] as a function of sound incidence angle, wind speed, and whitecap coverage. A first order, two-dimensional approach for bubble plume scattering [G] that includes the rough sea surface shows that bubble plume shadowing dominates the backscattered signal strength at shallow grazing angles. To demonstrate the effect, scale model experiments were performed at the Technical University of Denmark [H]. The scattered signal strength fluctuations observed at shallow angles are characteristic of the predicted ocean environment. Shadowing has a first order impact on the scattering strength observed from bubble plumes and clouds.

INTRODUCTION

The understanding of the impact of the sea surface ambient characteristics across a broad range of environmental conditions is critical. These influence underwater communications, environmental protection (observation of pollution of the sea), air-sea interaction (CO_2 transport across the sea surface), oceanography and other critical interaction driven processes. For the past several decades numerous experiments have been conducted to measure the ambient sea surface characteristics. For surface scattering the experimental observations and theory show reasonable agreement in the frequency range from a few kHz to ~ 60 kHz. Below a few kHz there are significant deviations between rough sea scattering predictions and experiments [F]. Scattering from bubble plumes and clouds generated by breaking waves has been proposed as an explanation for observed anomalies. The following sections provide a brief overview of the

experimental observations, proposed models, and the authors' research in developing an explanation for the experimental results.

The first section outlines the results from three sets of sea trials starting with the initial observations by Chapman and Harris [A] and Chapman and Scott [B] in the early 1960s, the deep water experiments conducted by Brown and Saenger [C], and the Critical Sea Test experiments as reported by Ogden and Erskine in the early 1990s [D,E]. The next section reviews theories proposed since the early 1990s to explain differences between observations in sea trials and rough sea surface scattering theories. Although models have been proposed to explain anomalous low frequency reverberation, disparities still exist between experimental data and predictions. The authors approach [G] for addressing these disparities includes scattering from bubble plumes that incorporates large-scale pressure release surface fluctuations and the impact of scattering center shadowing. Since shadowing appears to be a dominant contributor to observed backscattering signal strengths at shallow angles, the third section outlines scale model experiments conducted at the Technical University of Denmark to demonstrate this effect [H]. The experiments used a 1 MHz transducer as the source and receiver, a computer controlled data acquisition system, a scale model target, and a surface wave generator. The final section provides conclusions and areas for future research.

1. LOW FREQUENCY SEA SURFACE BACKSCATTERING EXPERIMENTS

In March, 1961 Chapman and Harris [A] conducted sea surface backscattering experiments in the deep-water basin near Bermuda. Using 1-pound TNT charges and an armored omni-directional hydrophone these trails measured backscattering from the rough sea surface. The fit to the experimental data developed by Chapman and Harris (Eq. 1) indicates that the scattering strength (SS) in dB as a function of wind speed, grazing angle, and frequency is within ± 3 dB of the data, as shown in Fig. 1.

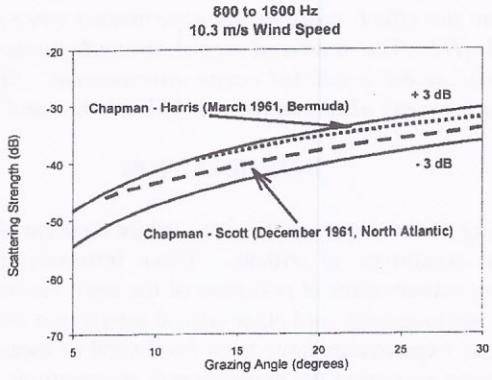

Figure 1. Measured backscattered signal strength versus prediction by Eq. 1.

$$SS = 3.3\beta \log\left(\frac{\theta}{30}\right) - 42.4\log(\beta) + 2.6 \qquad (1)$$

where $\beta = 158(vf^{1/3})^{-0.58}$, θ = grazing angle in degrees, v = wind speed in knots, and f = frequency in Hz.

In 1962, Brown and Saenger [C] conducted deep water bistatic reverberation experiments in the Caribbean Sea and the Virgin Island basin. The backscattering strength was measured in 1/2 octave bands from 62.5 to 4,000 Hz at wind speeds from 8 to 11 m/s. The experiments were conducted with 2.5 to 5 pound TNT equivalent charges. A conclusion drawn from the Brown and Saenger experiment is that bistatic scattering is influenced by surface shadowing of the incident signal.

In 1988 through 1991 the Critical Sea Test experiments were conducted in the Norwegian Basin, Icelandic Basic, Western Atlantic, Gulf of Australia, and the Ionian Basin [D,E]. The data was collected using broadband signal underwater sound (SUS) explosive charges as sources and a towed horizontal array as a collector. The test objective was to obtain data sets without limitations of the previous experiments. The backscattered signals were collected at grazing angles from 5° to 30°, wind speeds from 1.5 to 13.5 m/s, and wave heights from 0 to a few meters. There are two primary conclusions extracted from the CTS results shown in Fig. 2 [D]:

- Perturbation theory is adequate for calm seas and all wind speeds at lower frequencies
- For rougher seas and higher frequencies the Chapman-Harris curves adequately predict surface scattering

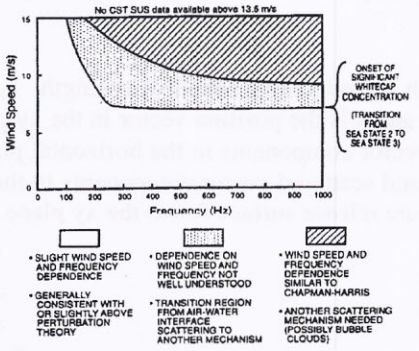

Figure 2. CTS results summary based on the data collected from all data sets.

2. ALTERNATIVE BACKSCATTERING THEORIES

Since the early 1990s several theories have been proposed to explain anomalous low frequency reverberation including:

- Scattering from late time bubble plumes with gas void fractions (β) ~ 10^{-6} using cylindrical plumes with ellipsoidal cross sections, B. McDonald [I], and circular cross sections, F. Henyey [J]
- Scattering from intermediate time bubble clouds with β ~ 10^{-2} to 10^{-4} with cloud shapes taken as spheres and ellipsoids, Gragg and Wurmser [K]
- Scattering from early to late time bubble structures with β ~ 10^{-2} to 10^{-6} with symmetrical and asymmetrical bubble plume and cloud shapes, Sakar and Prosperetti [L].

In each case the cloud/plume surface interactions assumed a planar pressure release surface. The complexity of the approaches ranges from the use of weak scattering theory to describe the interaction within the scattering volume [I,J] to the use of a T-matrix scattering approach [L]. For each approach there are regions where the agreement with Chapman and Harris' prediction is reasonable. However each approach has regions where the agreement deviates from the Chapman-Harris scattering strength formulation.

The simplest approach for bubble plume scattering is weak scattering theory (the Born approximation). When a breaking wave forms a bubble plume it creates a vertical near surface region of gas-entrained water. For plume depths up to 10 meters or more, as observed by high frequency backscattering data, the plume becomes a reverberation source. The entrapped gases change the sound speed within the plume, c, and the refraction index, n, where $c = c_o$ - *c, with c_o the ambient sound speed and *c the sound speed variation within the scattering volume. Based on weak scattering theory the scattering amplitude, f_s, and cross section per unit area, F, are given by

$$f_s = \frac{k_0^2}{\pi}\int K(r_0)e^{i(\bar{k}_{hi}-\bar{k}_{hs})\cdot\bar{x}_{hs}} \sin k_{zi} z \sin k_{zs} z dx dy dz \qquad \sigma = |f_s|^2 \qquad (2)$$

where k_o is $2\pi/\lambda$ with λ the incident sound wavelength, k_i is the incident wave vector, k_s is the scattered wave vector, and x is the position vector in the xy plane. The indices *hi* and *hs* refer to incident and scattered vector components in the horizontal plane, respectively, and the indices *zi* and *zs* refer to incident and scattered vector components in the vertical plane, respectively. As shown in Fig. 3, the pressure release surface forms the xy plane.

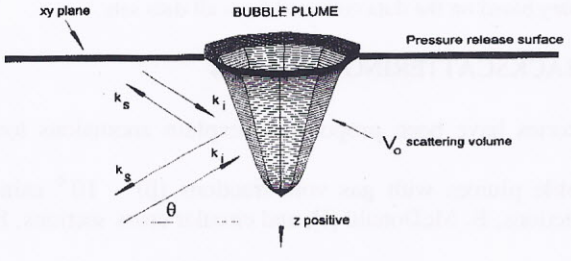

Figure 3. Scattering geometry

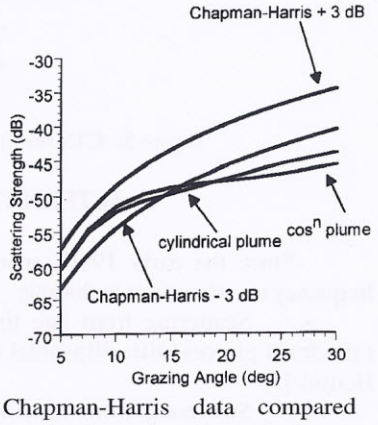

Figure 4. Chapman-Harris data compared to scattering from two alternative plume shapes

Fig. 4 compares the Chapman and Harris formulation and weak scattering theory bubble plume reverberation predictions when the late time bubble plume is ~ 8 meters in depth, ~ 1 m in radius, the U_{10} wind speed ~ 10 m/s, and the sound source is ~ 400 Hz. The void fraction when

the plume is modeled as a cylinder is ~ 2.6 x 10^{-6}, the plume shape is modeled a Cosine surface of revolution, the void fraction is ~ 2.2 x 10^{-6}, and the average e-folding depth for the void fraction is ~ 2.5 m. The backscattering strength (SS) is derived from McDonald's approximation [I]:

$$SS = 10\log\left(\frac{W(U_{10})\sigma}{plume\ surface\ area}\right) \tag{3}$$

where U_{10} is the wind speed in m/s at 10 m above the sea surface and $W(U_{10})$ the whitecap coverage [M] is given by

$$W(U_{10}) = 3.5\cdot10^{-3}\,(U_{10} - 3) + 4.2\cdot10^{-4}\,(U_{10} - 3)^2 \tag{4}$$

The agreement between predictions and the Chapman and Harris regression curves is reasonable at shallow grazing angles; however, results diverge beyond 15 degrees. An approach for enhancing the agreement is to remove the planar pressure release assumption from the scattering process.

3. BUBBLE PLUME SCATTERING INCLUDING SURFACE FLUCTUATIONS

As an approximation for scattering from bubble plumes when the pressure release surface is non-planar, the source, receiver, scattered pressure field, and surface corrugation are confined to the xz plane and the sea surface is assumed to be $g_s(x) = b[\cos(6\ x) - 1]$ where 6 given by $a/(1.2\ U_{10}^2)$ with a the acceleration due to gravity, U_{10} the wind speed (m/s), b the surface wave amplitude (m), and the bubble plume base is assumed attached to the corrugated surface. In the Born approximation the scattered amplitude $f(\theta_i)$ is given by:

$$f(\theta_i) = \frac{25000k_0^2}{4\pi}\iiint \varphi_0 e^{-i2k_0(x_1(x,z)\cos\theta_i + g_s(x_1(x,z))\sin\theta_i)} e^{-\frac{z-g_s(x_{plume})}{L}} \left(e^{i\varphi_s(x,z)+i\varphi_d(x,z)}\right)^2 dxdydz \tag{5}$$

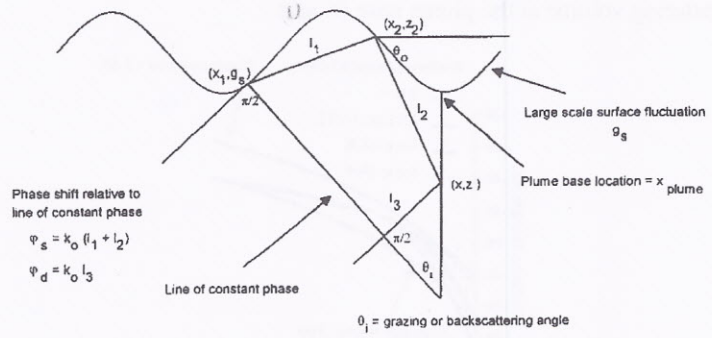

Figure 5. Surface Interaction Region.

The geometry of the scattering process is shown in Fig. 5, where x_1 and g_s are the x and z locations of the initial reflection on the surface that intersects the plume at the point (x,z), N_s is

the phase shift from the initial reflection point at (x_t, g_s) to the intersection at (x,z), N_d is the phase shift from the line of constant phase to the intersection at (x,z), and 2_i represents the grazing and backscattering angle. In the scattering integral, Eq. 5, the variation in the index of refraction accounts for the plume location on the non-planar pressure release surface and phase coherence is maintained between incident and scattered fields.

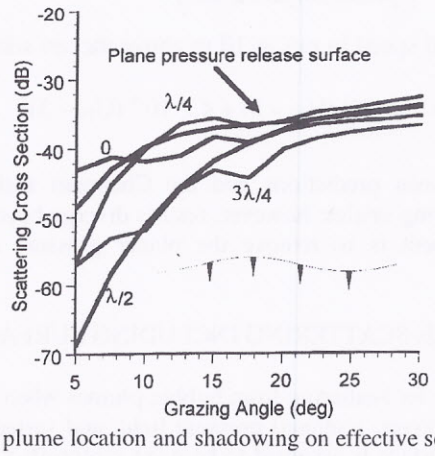

Figure 6. Impact of plume location and shadowing on effective scattering cross section

Fig. 6 illustrates the change in the scattering cross section when the bubble plume is at different locations on the rough sea surface. The calculations were performed for an average plume e-folding depth of 2.5 m, radius 1 m, length 8 m, and a cosine shaped scattering volume. In Fig. 6 the plume location is moved across a large scale fluctuation in increments of $8_s/4$. There is an ~30 dB change in the effective scattering cross section at shallow angles when the plume moves from the trough to the crest of the large scale surface fluctuation. As the bubble plume approaches the surface fluctuation's crest the shadowing by the preceding trough reduces the illuminated scattering volume at the plume base (z = 0).

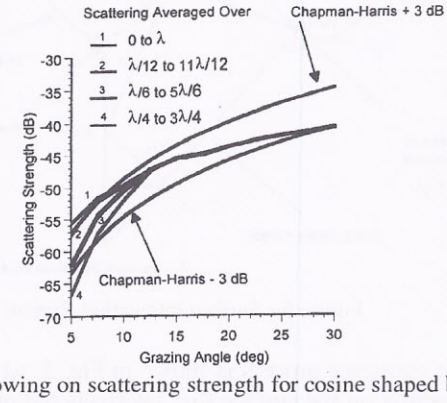

Figure 7. Impact of shadowing on scattering strength for cosine shaped bubble plume

Fig. 7 provides a comparison of the predicted scattering strength with the Chapman and Harris regression curves. In this instance the surface void fraction is on the order of $4x10^{-6}$, average void e-folding depth ~ 2.5 m, radius ~ 1 m, depth ~ 8 m, a cosine of revolution shape, incident sound frequency ~ 400 Hz, peak to peak wave height ~ 3.5 m, and surface wavelength ~ 77 m. Regardless of the location of the plumes on the large sea swells, the backscattering strength tends to follow the Chapman-Harris experimental regression curve. Scattering center shadowing is a dominant effect. Changes in the scattering center geometry have less of an effect on the magnitude. From a parametric study of the scattering cross section/scattering strength the following observations can be made:

- Shadowing effects decrease as the wave height decreases
- As the grazing angle increases the signal impinging on the scattering volume is focused and defocused
- As the plume depth increases the impact of shadowing decreases

4. SCALE MODEL EXPERIMENTS

To demonstrate shadowing impacts under controlled conditions a scale model experiment was conducted at the Technical University of Denmark [H]. The scaling was as follows: source frequency ~ 1 MHz (laboratory) vs ~ 1 kHz (ocean); wavelength ~ 77 m (ocean) to 10's cm (laboratory), peak-to-peak wave height ~ 3.5 m (ocean) vs ~ 0.01 m (laboratory), volume scattering (ocean) vs surface scattering (laboratory).

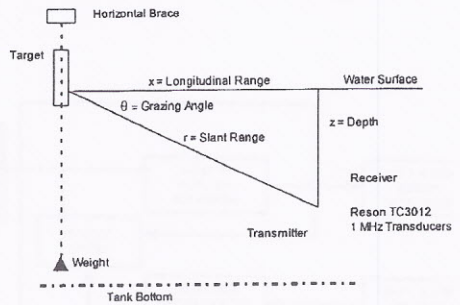

Figure 8. Scattering geometry

The tank's length, width, and height were 3 m, 1.5 m, and 1.5 m, respectively. A pneumatically driven wave generator formed 3 Hz surface waves with a wavelengths ~17.3 cm, velocities ~ 52 cm/sec, and peak-to-peak amplitudes that ranged between ~0.6 and ~1.2 cm. The target, located ~1.5 m from the wave generator, consisted of corks, with a ~ 2.3 cm diameter, a slight cylindrical taper or a hemispherical shape, and ~1 cm of the cork submerged. A nylon line attached to a horizontal brace across the tank was threaded through the cork center (Fig. 8) and attached to a weight suspended a few cm above the tank bottom. This constraining the cork

motion to the vertical direction. The interaction region was illuminated by a 1 MHz, 50 cycle pulse transmitted by a Reson TC3012 transducer aligned with the cork. The return signal was received by a second Reson TC3012 transducer. As shown by the calibration curve in Fig. 9 the transducers had a 1.5 cm diameter and a 3 dB beam width of 3 degrees. The transducers were mounted in a coplanar adapter with centers ~ 3.4 cm apart.

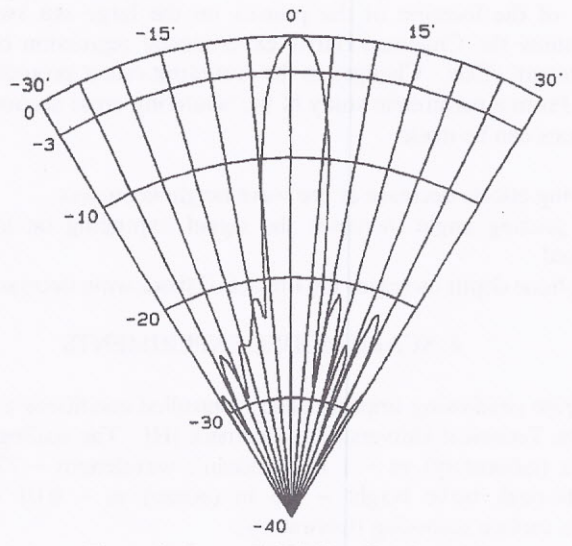

Figure 9. Reson TC3012 calibration data

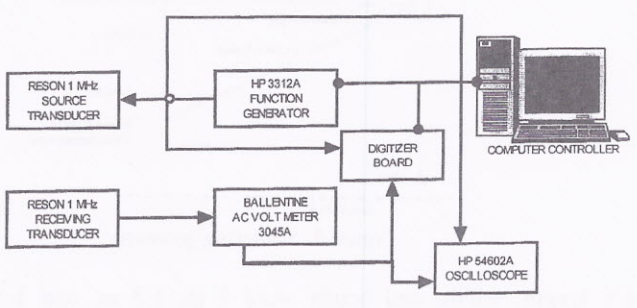

Figure 10. Data capture system block diagram

The computer controlled data acquisition system (Fig. 10) had five major subsystems: a Hewlett Packard 33120A signal generator, a Gage Applied Sciences Inc. CompuScope 225 data acquisition board, a Ballentine AC voltmeter, a HP 54602A oscilloscope, and a steering system with five stepping motors with control boxes. The data acquisition board had two channels with a 25 MHz sampling rate. The Ballentine AC voltmeter's wideband amplifier (5 Hz to 10 MHz) was used to amplify the backscattered signal. The signal generator, data acquisition board, and

transducer positioning were controlled by software developed by the Department of Industrial Acoustics. Stepping motors allowed motion along longitudinal (x) and transverse (y) directions in 0.0125 mm steps and along the z direction (vertical) in 0.00625 mm steps. Transducers were in an adapter connected to a gimbaled arm with two, stepping motor controlled, rotational axes - elevation (θ), step size 0.036^0 and azimuth (ϕ), step size 0.1^0.

Data was collected using a bistatic, pulse echo configuration at ranges from ~41.5 to ~ 52.8 cm and surface grazing angles (θ) from 5° to 15°. Multiple runs were collected automatically for a set of input parameters using the software control system. Given a series of inputs the software in a single file collected all data blocks for a single set using a fixed acquisition time window, performed the analog to digital conversion using the CompuScope data acquisition board, and stored the results on the hard drive. For each data acquisition 220 data blocks were collected with the target at rest at a fixed grazing angle. Next the wave generator was started, the system allowed to stabilize and 220 data blocks collected. Finally, the transducers were repositioned in x, z, and θ□□tank reverberation allowed to die out, and the process was repeated. The 50 cycle pulse's repetition rate was adjusted to minimize reverberation noise in the return signal's time window. At the start of data acquisition the source transducer's center was lined-up at the water level (0° grazing angle) with the target. The grazing angle was changed to 5° and the horizontal and vertical distances were set to maintain a constant range from the source to the target.

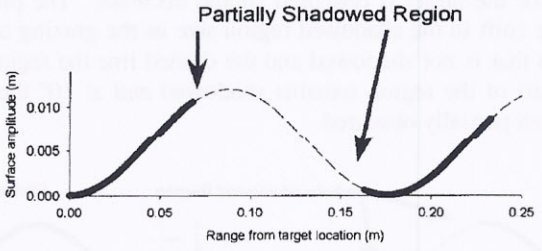

Figure 11. Surface shadowing at 5 degree grazing angle

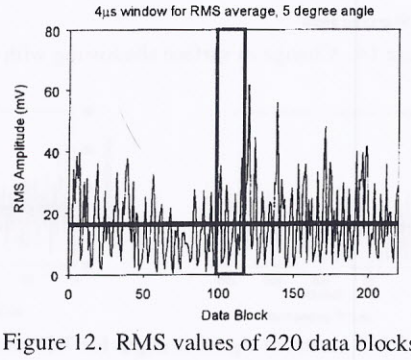

Figure 12. RMS values of 220 data blocks

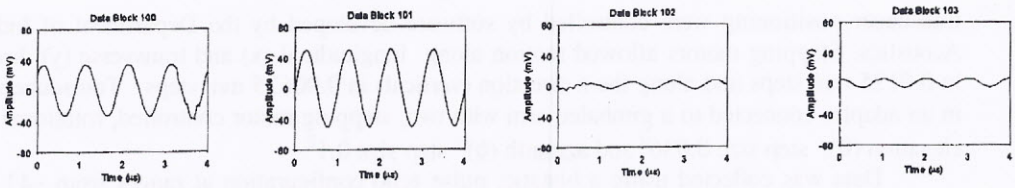

Figure 13. Individual data blocks from highlighted window shown in Fig. 12

Figure 11 is a plot of the surface wave starting at the target location. For a 5° grazing angle and the transducer located at 0.528 m the heavy line drawn on the surface is the region that is not shadowed and the dashed line is the region where the target is partially shadowed. Figure 12 is a plot of the root mean square (RMS) value of each of the 4 μs samples collected in a 220 set data block for the ~1.2 cm peak-to-peak wave height shown in Fig 11 and the transducer positioned at 5°. In this case the depth of the target in the water is ~ 1 cm. The horizontal line represents the average of the RMS values for the 220 sample data block. The fluctuations in the individual RMS values represent the target located at the wave crest (partially shadowed) to the target located at the wave trough (not shadowed). The variations between the 4 μs data blocks shown in Fig. 13 illustrates what happens when the target moves during the wave passage. For example, in data blocks 100 and 101 the target is barely obscured by the surface wave and in data blocks 102 and 103 the target is almost completely shadowed. As the grazing angle is increased the fraction of the time the target is obscured should decrease. The plot of the surface wave in Fig. 14 illustrates the shift in the shadowed region size as the grazing angle increases. The dark line shows the region that is not shadowed and the dashed line the region that is shadowed. At a 7.5° grazing angle part of the region remains shadowed and at 10° there is only a small region where the target is even partially obscured.

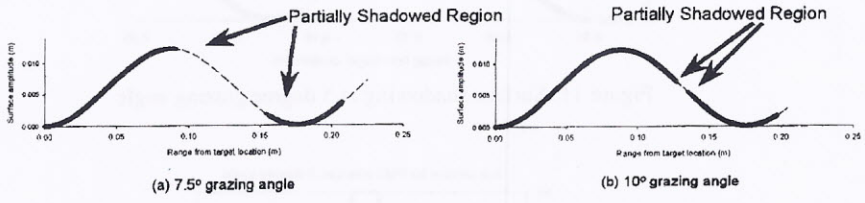

Figure 14. Change in surface shadowing with grazing angle

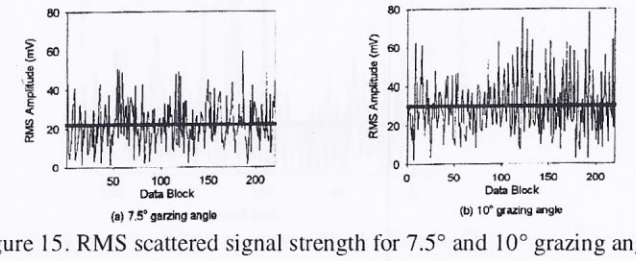

Figure 15. RMS scattered signal strength for 7.5° and 10° grazing angles

Figure 15 shows the RMS amplitude for a 4 μs sampling window as the grazing angle increases to 7.5° (Fig. 15a) and to 10° (Fig. 15b). As the grazing angle shifts from 5° (Fig. 11) to 7.5° and then to 10° less signal appears shadowed. This is consistent with the shift in the effective shadow zone shown in Figs. 11 and 14. The percentage of the area that is partially obscured shifts from approximately 60% to 40% to almost no obscuration. The RMS value over the entire data set is monotonically increasing and fewer and fewer of the individual data sets have near zero RMS amplitudes. When the grazing angle is increased to 10° shadowing ceases to be a contributor to the target's response. Other factors become dominant including surface wave induced focusing and defocusing of the signal on the target.

5. SUMMARY AND CONCLUSIONS

Observations from sea trials of low frequency sea surface reverberation in the few 100 Hz to few kHz frequency range show significant deviations from classical rough sea surface scattering predictions. Recent theories that attribute the increase in reverberation are consistent with bubble clouds or plumes acting as the scattering centers that produce the increased signal strength. However, the different approaches for bubble cloud and plume scattering have assumed that the ocean surface can be treated as a planar pressure release surface. When the sea surface fluctuations are incorporated into the scattering process, the agreement between bubble plume scattering and deep ocean measured signal scattering strength improves. The dominant mechanism is the shadowing of the bubble plume or cloud by the large scale sea surface fluctuations. Simple scale model experiments were able to provide a first order visualization of the key interactions under repeatable conditions and over large data samples. These experiments have demonstrated that scattering center shadowing produces a first order effect on the backscattered signal.

There are two clear challenges for future efforts. First, a more complex model of the scattering center/surface interaction should be developed. Moving from a two dimensional to a true three dimensional model should enhance the agreement between theory and experiment. Second, a higher fidelity scale model experiment should be developed to include multiple target interactions and enhanced target emulation.

ACKNOWLEDGEMENTS

The authors would like to acknowledge the support of the NATO Scientific Affairs Division and Science Applications International Corporation.

REFERENCES

1. R. P. Chapman and J. H. Harris, Surface backscattering strength measured with explosive sound sources, *J. Acoust Soc. Am.*, Vol. 34, 1592-1597, 1962.
2. *R. P.* Chapman and H. D. Scott, Surface backscattering strengths measured over an extended range of frequencies and grazing angles, *J. Acoust Soc. Am.*, Vol. 36, 1735-1737, 1964.

3. M. V. Brown and R. A. Saenger, Bistatic backscattering of low-frequency underwater sound from the ocean surface, *J. Acoust. Soc. Am.*, Vol. 52, 944-960, 1972.
4. P. M. Ogden and F. T. Erskine, Surface scattering measurements using broadband explosive charges in the Critical Sea Test experiments, *J. Acoust Soc. Am.,* Vol. 95, 746-761, 1994.
5. P. M. Ogden and F. T. Erskine, Surface and volume scattering measurements using broadband explosive charges in the Critical Sea Test 7 experiment, *J. Acoust Soc. Am.,* Vol. 95, 2908-2920, 1994.
6. S. T McDaniel., Sea surface reverberation: A review, *J. Acoust Soc. Am.,* Vol. 94, 1905-1922, 1993.
7. T. H. Neighbors and L Bjørnø, Low frequency sea surface reverberation, in *Underwater Acoustics*, J. S. Papadakis (Ed.), FORTH/IACM, Heraklion, Crete, Greece 1996.
8. T. H. Neighbors and L Bjørnø, Sea surface reverberation scale modeling, in Underwater Acoustics, A. Alippi and G. B. Cannelli (Eds.), Italian National Research Council, Rome, 1998.
9. B. E. McDonald, Echoes from vertically striated subresonant bubble clouds: a model for ocean surface reverberation, Vol. 89, *J. Acoust. Soc. Am.,* 617-622, 1991.
10. F. S. Henyey, Acoustic scattering from ocean microbubble plumes in the 100 Hz to 2 kHz region, Vol. 90, *J. Acoust. Soc. Am.*, 399-405, 1991.
11. R. F. Gragg and D. Wurmser, Low-frequency scattering from intermediate bubble plumes: Theory and computational parameter study, Vol. 94, *J. Acoust. Soc. Am.*, 319-329, 1993.
12. K. Sarkar and A. Prosperetti, Backscattering of underwater noise by bubble clouds, *J. Acoust. Soc. Am.*, Vol. 93, 3128-3138, 1993.
13. E. B. Kraus, *Atmosphere-Ocean Interaction*, Oxford University Press, New York, 1972.